# AIAA 95–0048

## Multigrid Unsteady Navier-Stokes Calculations with Aeroelastic Applications

Juan J. Alonso, Luigi Martinelli and Antony Jameson
*Princeton University, Princeton, NJ 08544*

**33rd AIAA Aerospace Sciences Meeting and Exhibit**
**January 9–12, 1995/Reno, NV**

**For permission to copy or republish, contact the American Institute of Aeronautics and Astronautics**
**1801 Alexander Bell Drive, Suite 500, Reston, VA 20191–4344**

AIAA 95–0048

# Multigrid Unsteady Navier-Stokes Calculations with Aeroelastic Applications

Juan J. Alonso,* Luigi Martinelli† and Antony Jameson‡
*Princeton University, Princeton, NJ 08544*

**An implicit approach to the solution of the unsteady two-dimensional Navier-Stokes equations is presented. After spatial discretization, the resulting set of coupled implicit non-linear equations is solved iteratively. This is accomplished using well proven convergence acceleration techniques for explicit schemes such as multigrid, residual averaging, and local time-stepping in order to achieve large computational efficiency in the calculation. Calculations are performed in parallel using a domain decomposition technique with optimized communication requirements. In addition, particular care is taken to minimize the effect of numerical dissipation with flux-limited dissipation schemes. Results for the unsteady shedding flow behind a circular cylinder and for a pitching NACA 64A010 airfoil are presented with experimental comparisons, showing the feasibility of accurate, efficient, time-dependent viscous calculations. Finally, a two-dimensional structural model of the cylinder is coupled with the unsteady flow solution, and time responses of the deflections of the structure are analyzed.**

## Nomenclature

| | |
|---|---|
| $C_l$ | coefficient of lift |
| $C_d$ | coefficient of drag |
| $C_x, C_y$ | damping coefficients in the two coordinate directions |
| $D$ | cylinder diameter, cylinder drag |
| $E$ | total energy (internal plus kinetic) |
| $\mathbf{E}(\mathbf{w}_{ij})$ | convective Euler fluxes |
| $\mathbf{f}, \mathbf{g}$ | Euler flux vectors |
| $H$ | total enthalpy |
| $K_x, K_y$ | spring constants in the two coordinate directions |
| $L$ | airfoil section lift (normal to free stream), positive up |
| $m$ | cylinder mass |
| $M_\infty$ | free stream Mach number |
| $n$ | frequency, $1/sec$ |
| $\mathbf{NS}(\mathbf{w}_{ij})$ | viscous flux residual for cell $i$,$j$ |
| $p$ | static pressure |
| $q_i$ | heat flux component |
| $\mathbf{R}(\mathbf{w}_{ij})$ | total flux residual for cell $i$,$j$ |
| $\mathbf{R}^*$ | modified residual |
| $\mathbf{R}, \mathbf{S}$ | viscous flux vectors |
| $Re_D$ | Reynolds number based on the diameter |
| $St$ | Strouhal frequency, $St = \frac{nD}{U_\infty}$ |
| $T$ | static temperature |
| $u, v$ | cartesian velocity components |
| $U_\infty$ | free stream velocity |
| $V_{ij}$ | volume of $i$,$j$ cell |
| $\mathbf{w}$ | vector of flow variables |
| $x_t, y_t$ | mesh cartesian velocity components |
| $\Delta\alpha$ | pitching motion forcing amplitude |
| $\Delta t$ | implicit real time step |
| $\gamma$ | ratio of specific heats, $\gamma = 1.4$ |
| $\rho$ | air density |
| $\sigma_{ij}$ | viscous stress tensor components |
| $\omega_f$ | frequency of the forced oscillations |
| $\Omega, \partial\Omega$ | cell element and boundary |

## Introduction

UNSTEADY flow solvers are becoming a necessary part of the toolkit of the computational fluid dynamicist. In order to solve problems which are naturally unsteady (such as vortex shedding flows, moving boundary problems, fluid-structure interaction flows, etc.) it is essential to develop numerical schemes which provide accurate solutions at a reasonable cost. Therefore, computational efficiency is of paramount importance for unsteady numerical solutions. As the governing equations increase in complexity (viscosity, turbulence, etc.), the computational efficiency of the method determines whether the approach can be useful as either an engineering or a research tool.

On the other hand, the solution of both inviscid and viscous steady flows can now be easily obtained, even for relatively complex geometries. This progress in the solution of steady flows has been closely coupled to the development of higher price/performance computing platforms, as well as to the appearance of very efficient numerical schemes and convergence acceleration techniques. Therefore it seems logical to make use of some of these techniques that have proven successful in the solution of steady flows, and apply them to the calculation of time dependent flows.

*Graduate Student, AIAA Member
†Assistant Professor, AIAA Member
‡James S. McDonnell Distinguished University Professor of Aerospace Engineering, AIAA Fellow

Copyright © 1995 by the authors. Published by the American Institute of Aeronautics and Astronautics, Inc. with permission.

Explicit time accurate methods must advance all cells in the computational domain with the same time step to maintain consistency. The global time step is therefore limited by the most restrictive of the allowable time steps in the domain. Unfortunately, due to the Courant-Friedrichs-Levy (CFL) restriction, this can lead to a very large number of time steps in order to complete a calculation. Unless the frequency of the physical phenomena that we want to resolve is of the order of the characteristic frequencies of acoustic disturbances, such a choice of the time step is based on the stability of the numerical scheme, and not on issues of accuracy of the solution of the problem of interest. Therefore, we see ourselves forced to choose a time-step that is quite a bit smaller than the one we would require to ensure accuracy, with a consequent increase in the time of computation.

If the problem is formulated in an implicit fashion, this explicit time step limitation can be bypassed. Moreover, at each time step, the implicit set of equations which results from the discretization of the governing equations of the flow can be cast as a modified steady-state problem in pseudo-time. Then, efficient techniques such as multigrid and residual averaging can be applied without sacrificing time accuracy, and great improvements in computational performance can be achieved.

Brenneis and Eberle[1] solved the unsteady two- and three-dimensional implicit unfactored Euler equations by using a non-linear Newton method and a Gauss-Seidel algorithm for relaxation purposes. They used a first order accurate discretization of the time derivative operator which allowed them to use on the order of fifty to one hundred time steps per cycle of oscillation of the physical phenomena in question.

Jameson[2] used a second order backwards difference operator for the time derivative term, and applied multigrid and residual averaging to the solution of the implicit system. With this approach he was able to solve unsteady flows about two- and three-dimensional configurations in twenty to thirty time steps per cycle of oscillation. Later, this method was shown to work well for a third order accurate stiffly stable backwards difference formula, as well as for aeroelastic calculations.[3] With this discretization, only fifteen steps per period of oscillation are necessary to ensure an accurate solution.

It has become clear that inviscid models yield a cost effective approximation to the solution of unsteady problems, but when strong shocks and separated flows are involved, it is necessary to incorporate viscosity and turbulence effects into the model.[2,5] Especially in transonic flows where shocks are present, there is a tendency of inviscid models to overpredict the strength of the shock, and to place the location of these shocks slightly aft of the experimental location.[1] With this perspective in mind it is only natural to think of applying a similar approach to that of Jameson[2] to the solution of the unsteady Navier-Stokes equations. In this case, the explicit time-step restrictions are even less tolerable, since the ratio of the maximum to the minimum size of the cells in a viscous mesh can span several orders of magnitude. This means that the gains to be obtained from an implicit method are even more substantial than those reported for the Euler equations. Melson et al.[4] applied Jameson's approach to the solution of the unsteady Thin Layer Navier-Stokes equations and pointed out the possible gain in robustness of the algorithm when some terms are treated implicitly in the Runge-Kutta time-stepping. Arnone et al.[5,6] followed the same approach and computed flows over rows of cylinders, bicircular arc airfoils, and turbomachinery flows at subsonic and transonic Mach numbers with very promising results.

In this work we present a similar approach applied to the solution of the full Navier-Stokes equations,[8,9] where all these improvements to the convergence of the method have been incorporated to the scheme, and various flux-limited dissipation schemes are evaluated.[7] Vortex shedding flows over stationary and oscillating cylinders in an infinite free stream are calculated, as well as the unsteady flow over a pitching NACA 64A010 airfoil. Experimental comparison of the unsteady lift coefficient for the NACA 64A010 airfoil is shown, and preliminary results of the aeroelastic coupling of the flow over a cylinder with a two-dimensional model of the structure are also presented.

## Navier-Stokes Equations and Discretization

The two-dimensional unsteady compressible Navier-Stokes equations, after the appropriate non-dimensionalizations, can be written in a cartesian coordinate system $(x, y)$ as:

$$\frac{\partial \mathbf{w}}{\partial t} + \frac{\partial \mathbf{f}}{\partial x} + \frac{\partial \mathbf{g}}{\partial y} = \left( \frac{\partial \mathbf{R}}{\partial x} + \frac{\partial \mathbf{S}}{\partial y} \right), \qquad (1)$$

where $\mathbf{w}$ is the vector of flow variables, $\mathbf{f}$ and $\mathbf{g}$ are the convective flux vectors, and $\mathbf{R}$ and $\mathbf{S}$ are the viscous flux vectors in each of the coordinate directions. Consider a control volume $\Omega$ with boundary $\partial\Omega$ which moves with cartesian velocity components $x_t$ and $y_t$. The equations of motion of the fluid can then be written in integral form as

$$\begin{aligned} \frac{d}{dt} \iint_{\Omega} \mathbf{w} \, dx \, dy \quad + \quad & \oint_{\partial\Omega} (\mathbf{f} \, dy - \mathbf{g} \, dx) = \\ = \quad & \oint_{\partial\Omega} (\mathbf{R} \, dy - \mathbf{S} \, dx), \end{aligned} \qquad (2)$$

where $\mathbf{w}$ is the vector of flow variables

$$\mathbf{w} = \left\{ \begin{array}{c} \rho \\ \rho u \\ \rho v \\ \rho E \end{array} \right\},$$

$\mathbf{f}$, $\mathbf{g}$ are the Euler flux vectors

$$\mathbf{f} = \left\{ \begin{array}{c} \rho(u - x_t) \\ \rho u(u - x_t) + p \\ \rho v(u - x_t) \\ \rho E(u - x_t) + pu \end{array} \right\}, \mathbf{g} = \left\{ \begin{array}{c} \rho(v - y_t) \\ \rho u(v - y_t) \\ \rho v(v - y_t) + p \\ \rho E(v - y_t) + pv \end{array} \right\},$$

and

$$\mathbf{R} = \left\{ \begin{array}{c} 0 \\ \sigma_{xx} \\ \sigma_{xy} \\ u\sigma_{xx} + v\sigma_{xy} - q_x \end{array} \right\},$$

$$\mathbf{S} = \left\{ \begin{array}{c} 0 \\ \sigma_{xy} \\ \sigma_{yy} \\ u\sigma_{xy} + v\sigma_{yy} + q_y \end{array} \right\}$$

are the viscous flux vectors, where the stress tensor components and the heat flux vector are given by

$$\begin{aligned} \sigma_{xx} &= 2\mu u_x - \frac{2}{3}\mu(u_x + v_y) \\ \sigma_{yy} &= 2\mu v_y - \frac{2}{3}\mu(u_x + v_y) \\ \sigma_{xy} &= \sigma_{yx} = \mu(u_y + v_x) \\ q_x &= -\kappa \frac{\partial T}{\partial x} \\ q_y &= -\kappa \frac{\partial T}{\partial y}. \end{aligned}$$

The coefficient of viscosity, $\mu$, is calculated according to Sutherland's law. Also, for an ideal gas, the equation of state may be written as

$$p = (\gamma - 1)\ \rho\ \left[ E - \frac{1}{2}(u^2 + v^2) \right].$$

Turbulence effects can be taken into account by use of a suitable turbulence model. In this work, a Baldwin-Lomax algebraic turbulence model[11] has been used when necessary. Details of the implementation can be found in[9] and.[10] When the integral governing equations (2) are applied independently to each cell in the domain, we obtain a set of coupled ordinary differential equations of the form

$$\frac{d}{dt}(\mathbf{w}_{ij}\, V_{ij}) + \mathbf{E}(\mathbf{w}_{ij}) + \mathbf{NS}(\mathbf{w}_{ij}) + \mathbf{D}(\mathbf{w}_{ij}) = \mathbf{0}, \quad (3)$$

where $\mathbf{E}(\mathbf{w}_{ij})$ are the convective Euler fluxes, $\mathbf{NS}(\mathbf{w}_{ij})$ are the Navier-Stokes viscous fluxes, and $\mathbf{D}(\mathbf{w}_{ij})$ are the artificial dissipation fluxes added for numerical stability reasons. This equation (3) can be discretized implicitly as follows (drop the $i, j$ subscripts for clarity):

$$\frac{d}{dt}[\mathbf{w}^{n+1}\, V^{n+1}] + \mathbf{R}(\mathbf{w}^{n+1}) = \mathbf{0}, \quad (4)$$

where $\mathbf{R}$ is the sum of the three flux contributions, and the superscripts denote the time step of the calculation. If we discretize the time derivative term with, say, a backwards difference second order accurate operator, we obtain

$$\begin{aligned} \frac{3}{2\Delta t}[\mathbf{w}^{n+1}V^{n+1}] &- \frac{2}{\Delta t}[\mathbf{w}^{n}V^{n}] + \frac{1}{2\Delta t}[\mathbf{w}^{n-1}V^{n-1}] \\ &+ \mathbf{R}(\mathbf{w}^{n+1}) = \mathbf{0}. \end{aligned} \quad (5)$$

This equation for $\mathbf{w}^{n+1}$ is non-linear due to the presence of the $\mathbf{R}(\mathbf{w}^{n+1})$ term and cannot be solved directly. One must therefore resort to iterative methods in order to obtain the solution. The time integration of the Navier-Stokes equations at each time step can then be seen as a modified pseudo-time steady-state problem with a slightly altered residual

$$\begin{aligned} \mathbf{R}^*(\mathbf{w}) &= \frac{3}{2\Delta t}[\mathbf{w}\, V^{n+1}] - \frac{2}{\Delta t}[\mathbf{w}^{n}V^{n}] \\ &+ \frac{1}{2\Delta t}[\mathbf{w}^{n-1}V^{n-1}] + \mathbf{R}(\mathbf{w}). \end{aligned}$$

In this case, the vector of flow variables $\mathbf{w}$ which satisfies the equation $\mathbf{R}^*(\mathbf{w}) = \mathbf{0}$ is the $\mathbf{w}^{(n+1)}$ vector we are looking for. In order to obtain this solution vector, we can reformulate the problem at *each* time step as the following modified steady-state problem in a fictitious time, $t^*$:

$$\frac{d\mathbf{w}}{dt^*} + \mathbf{R}^*(\mathbf{w}) = \mathbf{0}, \quad (6)$$

to which one can apply the fast convergence techniques used for steady-state calculations. Applying this process repeatedly, one can advance the flow field solution forward in time in a very efficient fashion. The reader is referred to[2] for a more complete description of the approach.

In this work, a third order accurate discretization of the time derivative operator has been used in all cases. When applied to the model one-dimensional problem, this discretization is stiffly stable, but due to the presence of viscous fluxes, this slight restriction does not present practical problems. When a Fourier analysis for the model one-dimensional equation is performed, it is seen that the Fourier symbol of the residual shifts in the negative direction of the real axis by an amount which is proportional to the pseudo-time step in each cell, $\Delta t^*$, with a proportionality constant that depends on the order of accuracy of the time discretization. There exists the possibility, for the large cells in the domain (where $\Delta t^*$ is large), that the numerical scheme will become unstable. In the original code, the time step was cut off at a given

level in order to restrict the shifting of the Fourier symbol of the residual out of the stability region of the Runge-Kutta time-stepping scheme. The proportionality constant becomes larger as the order of accuracy of the time discretization increases, and curiously, as the real time step $\Delta t$ decreases. Melson et al.[4] treated the $\frac{3}{2\Delta t}[\mathbf{w}\, V^{n+1}]$ term implicitly in the Runge-Kutta time-stepping. In this case, the one-dimensional analysis indicates the disappearance of the stability problem in the larger cells of the domain, and a possible decrease in the amplification factor for all frequencies. In a sense, their approach is equivalent to a rescaling of the pseudo-time step for every cell in the domain, and, in practice, does not lead to noticeable improvements in convergence. Nevertheless, this change in the algorithm increases considerably the robustness of the method, and eliminates the need of an extra parameter. Therefore, it has been adopted in our code.

## Numerical Dissipation

The calculation of compressible flows at transonic and supersonic Mach numbers requires the implementation of non-oscillatory discrete schemes which combine high accuracy with high resolution of shock waves and contact discontinuities. These schemes must also be formulated in such a way that they facilitate the treatment of complex geometric shapes. When dealing with viscous flows, care must be taken in order not to spoil the accurate resolution of the viscous phenomena. The difficulty rests on the fact that shock capturing requires the construction of schemes which are *numerically* dissipative, a requirement which could affect the global accuracy of the solution of the *physical* viscous problem.

In a recent paper,[7] starting from the local extremum diminishing (LED) principle proposed by Jameson,[12] the accuracy of a large family of schemes, comprising both high resolution switched and flux-limited dissipation schemes, has been evaluated for viscous solutions. In particular, both symmetric limited positive (SLIP), and upstream limited positive (USLIP) schemes, were found to yield very accurate resolution of laminar boundary layers on a wide range of Mach and Reynolds numbers.

More recently, a new approach to the formulation of the artificial dissipation which combines sharp resolution of discontinuities with good accuracy in boundary layers and wakes has been proposed.[13] This new approach has been denominated H-CUSP, and was used in this paper. Validation for steady viscous flows and a description of the scheme can be found in an accompanying paper.[25]

One of the objectives of the present work is to investigate the validity of the H-CUSP scheme for unsteady viscous flows with moving shock waves.

## Aeroelastic Model

The model used in these initial calculations is similar to the typical section wing model widely used in aeroelastic calculations.[14,15] In this case, instead of having a torsional spring to model the pitching deflection of the wing, the cylinder is connected to two linear springs along each of the coordinate axes. Since both $C_l$ and $C_d$ are functions of time, displacements in both coordinate directions will be excited by the unsteadiness in the flow.

The governing equations of the structural model are simply:

$$\begin{aligned} m\ddot{x} + C_x\dot{x} + K_x x &= L \\ m\ddot{y} + C_y\dot{y} + K_y y &= D, \end{aligned}$$

where $L$ and $D$ are the lift and the drag of the cylinder respectively, $m$ is the mass of the cylinder, $C_x$ and $C_y$ are the damping coefficients of the dampers, and $K_x$ and $K_y$ are the spring constants of the horizontal and vertical springs (all of which can be seen in Figure 1). These equations are already in modal form (since they are fully uncoupled), and can be solved implicitly using the approach in.[3] This approach involves the decomposition of each of these modal equations into a system of first order differential equations which is later diagonalized and integrated in time with a Runge-Kutta approach. The reader is referred to[3] for more details on this procedure.

The structural model is coupled to the Navier-Stokes equations in the pseudo-time steady-state calculation for each time step. This coupling is fully implicit, and therefore, at the end of each pseudo-time iteration, both systems of equations are in full agreement with each other. The cylinder is held in place until the vortex shedding flow pattern is fully developed, and is then released and left to evolve due to its own self-induced forces.

The complete model is supposed to represent the first bending mode in both coordinate directions of a long cable in water or air, which is a relevant problem for both marine structures and civil engineering problems.[17]

## Parallelization Strategy

Increasingly complex fluid flow models require high performance computing facilities. A cost effective solution for problems of this type requiring fast CPU's and large internal memory is the use of a parallel computing paradigm. For numerical efficiency, one typically incorporates convergence acceleration techniques such as multigrid and implicit residual smoothing. Message passing becomes necessary in this new environment, and severely limits the performance of processes that are inherently communication intensive.

UFLO82NSP is parallelized using a domain decomposition model, a SPMD (Single Program Multiple

Data) strategy, and the MPI (Message Passing Interface Standard) Library for message passing.[19] Flows were typically computed on an O-mesh of size $n_i \times n_j = 384 \times 96$. This domain was decomposed into subdomains containing $\frac{n_i}{N_p} \times n_j$ points, where $N_p$ is the number of subdomains used. Communication between subdomains was performed through halo cells surrounding each subdomain boundary. A two-level halo was sufficient to calculate the convective, viscous, and dissipative fluxes in the finest mesh of the cycle. In the coarser levels of the multigrid cycle, a single level halo suffices.

For problems with a low task granularity (ratio of the number of bytes received by a processor to the number of floating point operations it performs), large parallel efficiencies can be obtained. Unfortunately, convergence acceleration techniques developed in the 1980s base their success on global communication in the computational domain. Thus, current multigrid and especially implicit residual smoothing techniques hinder parallel performance. Nevertheless, one can effectively deal with these issues by modifying the algorithm to minimize the amount of messages passed. Several techniques to deal with the parallelization of multigrid and implicit residual smoothing were described in.[20] In particular, the usage of an iterative approach for the implicit residual averaging, restores parallel efficiencies to a level around 90% for 8 processors.

With this and other improvements incorporated to the parallel version of the code, the unsteady computations in this work can be carried out in a small amount of time, which allows for almost interactive parameter studies, as well as continuous feedback on the computations.

Parallel benchmarks were performed on an IBM SP2 platform with up to 8 processors. In Figure 2, we can see the parallel speedup curves for the full code, including multigrid and residual averaging, for two different message passing implementations on the IBM SP1 and SP2 distributed memory machines. For these structured meshes, the domain decomposition is straightforward, and nearly perfect load balance is achieved. For the size of the meshes used in this study, parallel performance starts to drop off for 12 or more processors, since the amount of computations that each processor performs becomes offset by the increasing amount of communication required by a larger number of processors.

For illustration purposes, Figure 3 shows the Mach number contours on a NACA 64A010 airfoil at 2° angle of attack, and $Re_\infty = 5000$, with the processor boundaries being the nearly radial coordinate emanating from the airfoil. This calculation used 12 processors. The continuity of the Mach number contour lines is an indicative of the quality of the parallel solution.

## Results and Discussion

This section is divided according to the type of computations performed. First, we will show the results for the simulation of the vortex shedding flow over a circular cylinder at a Reynolds number $Re_D = 500$. Experimental investigations[21–23] show that a laminar, two-dimensional wake exists in the Reynolds number range $40 - 180$. After that, the wake becomes three-dimensional. In the first section we are only interested in the properties of the numerical scheme. Therefore, the fact that the real flow is three-dimensional is of no consequence. Secondly, we will show the results for the unsteady transonic flow over a pitching NACA 64A010 airfoil and compare it to experimental data. Finally, aeroelastic calculations for a structural model of a circular cylinder are carried out, and comparisons of the maximum oscillation amplitude with experimental data are presented.

### Vortex shedding over a circular cylinder at $Re_D = 500$

In order to test the accuracy of the baseline code, we chose a problem that is well documented both experimentally and numerically, such that meaningful comparisons of the computed solutions were possible. Initially, we investigated the problem of vortex shedding behind a circular cylinder. It is well known[16] that in the Reynolds number range from 40 to 5000, a regular Kármán vortex street is observed. In this range, the Strouhal frequency of vortex shedding, $St = \frac{n\,D}{U_\infty}$, where $n$ is the real frequency, $D$ is the diameter of the cylinder, and $U_\infty$ is the free stream velocity, is only a function of the Reynolds number.

We set out to perform a refinement study in both space and time in order to determine the minimum resolutions that must be used if one wants to have fully resolved calculations. During these studies, the Reynolds number was fixed at $Re_D = 500$, the Mach number for the computation was $M_\infty = 0.20$ (which is very nearly incompressible flow), and the far field boundary of the mesh was fixed at 50 cylinder diameters. In Figure 4, we can see a detail of the inner part of the grid used in this calculation. In the $384 \times 96$ mesh, about 32 cells were placed in the boundary layer in order to fully resolve the effects of the presence of the solid wall. The mesh stretches geometrically from the surface of the cylinder in order to cluster the points near the solid surface. At the solid wall, the no-slip kinematic condition is imposed. The wall is also considered to be adiabatic. In the far field, inviscid, non-reflecting boundary conditions are used.[27] Due to the symmetry of the code and the initial conditions, vortex shedding can only be caused by roundoff error in the simulation. This was proven to be true in one of the initial simulations. However, in order to avoid unnecessary waste of computational time, the cylinder was forced in pitch for one cycle of amplitude

$\Delta\alpha = 1°$, at a frequency, $\omega_f$, close to the vortex shedding frequency. After this forced cycle, the cylinder remains stationary for the rest of the calculation. The flow slowly develops an asymmetric instability, and alternate shedding proceeds in a periodic fashion. In Figure 5, we can see the typical development of the periodic response in the coefficients of lift and drag. Notice the small notch produced by the sudden cease in the forced motion of the cylinder. After the flow is forced, the strength of the shed vortices increases until it reaches a limit amplitude in both $C_l$ and $C_d$. Notice as well that the frequency of the coefficient of drag is twice that of the coefficient of lift due to symmetry considerations. Figure 10 shows the instantaneous streamlines at three different times in the shedding cycle once periodicity has fully developed, and one can clearly see the process by which the separating boundary layer feeds vorticity into the vortex that is about to be shed. Finally, in Figure 6, we can see the first four vortices that are captured before the grid coarsens beyond the point where an accurate solution can be obtained.

Four meshes were used in the grid refinement study conducted for this flow. The sizes of these meshes were: $96 \times 24$, $192 \times 48$, $384 \times 96$, and $384 \times 192$. The first two meshes (as we can see in Figure 7) do not provide the appropriate resolution of the viscous phenomena. The added viscosity (in the form of artificial dissipation introduced by the numerical scheme) retards the development of the shedding, and limits the peak to peak variation of the coefficient of lift, while increasing the coefficient of drag. The flows in the following two meshes exhibit a slight difference in the time to develop the full vortex shedding motion, but, as we can see in Table 1, the differences in the Strouhal frequency of shedding, and the $C_l$ amplitude are on the order of one half of a percent. Apart from the small difference in phase, it was considered that the $384 \times 96$ mesh provided the necessary accuracy for the solution of this type of flows, and therefore, all the subsequent calculations in this paper are performed in meshes of these dimensions. All calculations in this mesh refinement study were done with 20 time steps per period of oscillation of the lift coefficient. Due to the bunching of the cells close to the surface of the cylinder, Courant numbers of the order of $50,000$ and higher can be achieved in these calculations with the implicit time stepping scheme. Thus, the implicit scheme can be of the order of one thousand times more efficient than an explicit scheme, which could only achieve comparable accuracy at prohibitive computational costs. The calculated Strouhal frequency was $St = 0.231$, which agrees quite well with the experimental value of 0.235 extrapolated from the curves for incompressible flow in the laminar shedding regime.

In order to verify the properties of the discretization of the time derivative operator, we conducted a study

| Mesh Size | $St_{C_l}$ | $C_{l_{max}}$ | $C_{d_{avg}}$ | $St_{C_d}$ |
|---|---|---|---|---|
| $96 \times 24$ | 0.13384 | 0.05624 | 0.68857 | 0.27292 |
| $192 \times 48$ | 0.22466 | 0.87248 | 1.10768 | 0.44981 |
| $384 \times 96$ | 0.23313 | 1.14946 | 1.31523 | 0.46735 |
| $384 \times 192$ | 0.23103 | 1.14671 | 1.35923 | 0.46868 |

**Table 1 Relevant Quantities in the Spatial Grid Refinement Study**

| Time steps per period | $St_{C_l}$ | $C_{l_{max}}$ | $C_{d_{avg}}$ | $St_{C_d}$ |
|---|---|---|---|---|
| 10 | 0.22812 | 0.92011 | 1.24888 | 0.45698 |
| 20 | 0.23313 | 1.14946 | 1.31523 | 0.46735 |
| 30 | 0.22320 | 1.06801 | 1.22030 | 0.44669 |
| 40 | 0.22469 | 1.04562 | 1.21759 | 0.44878 |
| 50 | 0.22470 | 1.04560 | 1.21723 | 0.44923 |

**Table 2 Relevant Quantities in the Time Step Refinement Study.**

which used 10, 20, 30, 40, and 50 time steps per cycle of oscillation of the lift coefficient for the same parameters in the problem above. The size of the mesh used in this study was $384 \times 96$. The same procedure was followed to force the flow into its periodic solution. Figure 8 shows the time history of $C_l$ for the calculations with 10, 20, 30, and 40 time steps per period after the shedding motion is fully developed. The results for 50 time steps per period are omitted since they coincided exactly with those for 40 time steps per period, and would make the figure less readable. The results for 30 and 40 time steps per period are in very good agreement except for a slight difference in phase. In Table 2, we see that the Strouhal frequency of shedding differs by 0.6% for these last two cases. It was therefore estimated that a number of time steps between 30 and 40 is sufficient to ensure a very accurate solution. With this in mind, the simulations in the following sections used 36 time steps per period of oscillation of the meaningful quantities. All these calculations have been made with a third order accurate discretization of the time derivative term. While the third order discretization requires the storage of an extra level of the grid and flow variables, the number of time steps per period that are necessary is smaller, thus making it more computationally efficient. It is believed that the tradeoff between computational efficiency and memory storage might favor the second order scheme for viscous three-dimensional calculations.

**Pitching NACA 64A010 Airfoil**

One of the advantages of the current formulation is that it can be applied to the whole Mach number range. The algorithm discussed in this paper covers the compressible regime (subsonic, transonic, and supersonic), whereas an accompanying paper[18] discusses the implementation of an artificial compressibility method for truly incompressible flows. Moreover, the algorithm is valid for complex configurations, and

one needs not be limited to the solution of flows over a cylinder. Our area of interest is mainly in transonic flows, and therefore, we wanted to compute the unsteady flow over a pitching airfoil, in this case a NACA 64A010 airfoil. In the case of turbulent calculations, explicit methods become unaffordably expensive, and the current method can really be of help.

In the past,[2] the inviscid flow over this airfoil has been calculated, and the unsteady $C_l$ vs. $\alpha$ curve was found to agree quite well with the experiment. The experimental results lie on a periodic curve in the shape of an oval, which is slightly broader than the inviscid calculations. In Figure 9 we can see that the inclusion of viscous effects tilts the inviscid oval in the direction of the experimental results. The very slight difference still existing can be due to inaccuracies in the turbulence model. For attached flows, we can conclude that inviscid solutions are the best compromise for the prediction of lift related properties. However, if in addition one wants to obtain drag and pitching moment information, the only option is to use the full Navier-Stokes equations with a suitable turbulence model. Figure 11 shows the motion of the shocks in the upper and lower surfaces of the airfoil for a little more than half a pitching cycle. The snapshots are arranged by rows. As the airfoil pitches up, the shock in the upper surface moves aft at the same time as it becomes stronger. The shock in the lower surface moves forward, weakens, and disappears. As the airfoil pitches down, the opposite begins to happen, with a small phase lag. By virtue of the usage of the improved dissipation constructions (H-CUSP in this case) in Section , shocks can be resolved very crisply, with the additional advantage that the actual viscosity in the flow field is contaminated to a much lesser degree. Finally, Figure 12 shows the coefficient of pressure along a coordinate line that circles the airfoil right outside of the boundary layer. One can clearly see that these the results, which were obtained with the H-CUSP scheme, are by all means superior to the ones that could be obtained with a scalar dissipation model which spreads the shock over 4 or 5 cells instead of 1 or 2.

**Preliminary Aeroelastic Calculations for a Circular Cylinder**

In this section we present preliminary calculations of an aeroelastic model of a circular cylinder in a free stream with the motion induced by its own aerodynamic forces. The details of the model, which has very simple governing equations of motion, are shown in Figure 1. This model has been previously tested with a Galerkin spectral formulation by Blackburn et al.[17] As the computation proceeds, vortex shedding occurs and the motion of the structure is dictated by the variation in time of the force coefficients. The Reynolds number of the flow is once more $Re_D = 500$, the dimensions of the mesh are $384 \times 96$, and the time step is taken such that it corresponds to 1/36 of the period dictated by a Strouhal number $St = 0.2$. The cylinder is given an initial displacement and velocity in the y coordinate direction, and after 5 time steps, it is allowed to evolve due to its own self-induced forces. The cylinder mass ratio is taken to be $\mu = 5.0$ for all cases, and the natural frequency of the springs is chosen to match the same Strouhal number $St = 0.2$. The damping coefficient of the springs is varied to compare with experimental data. It is clear that if the motion of the cylinder did not considerably affect the force coefficients, the amplitude of the oscillations would increase without bound. In reality this is not so, and, as the cylinder moves, the lift force is limited, preventing the vertical displacement from becoming infinite. Nevertheless, comparisons between the force coefficients obtained during free and forced vibrations can still provide very beneficial insights. First of all, in Figure 13, we present the results of a typical calculation in which the reduced damping[17] ($\frac{\zeta}{\mu} = 8\pi^2 St^2 m\zeta/\rho_\infty D$) is 5.0 (the reduced damping is a parameter that coalesces the spring damping coefficient and the cylinder mass ratio). This figure clearly resembles the evolution of $C_l$ and $C_d$ for the stationary cylinder in the previous section. The vertical motion is centered about the starting position, whereas the horizontal motion has an average positive displacement due to the existence of a net drag. If the reduced damping is decreased to 1.0, the amplitude of the vertical motion increases (as one would expect, since more of the energy transferred from the fluid into the structure is used in storing potential energy in the spring, and a smaller part of it is dissipated in the dampers). Figure 14 shows a phase plot of the time accurate trajectory of the center of our cylinder. It can be seen that the motion slowly develops into a periodic orbit centered about the vertical origin and displaced to the right by an amount proportional to the drag coefficient. Notice the fact that the periodic orbit is in the shape of a figure-eight, since the frequency of the horizontal forcing (drag) is twice that of the vertical one (lift).

When one varies the reduced damping for the same conditions, the maximum vertical displacement of the cylinder varies accordingly. Griffin[24] has compiled a set of experimental data for this type of flows, for widely varying Reynolds Numbers ($300 < Re_D < 10^6$). Blackburn and Karniadakis[17] have performed similar computations, and all these results, together with those obtained by the current method, are presented in Figure 15. One can see that although the Reynolds number of the data is, in general, not matched with that of the computation, the trend is captured quite reasonably, and the maximum amplitude of the motion can be predicted quite accurately in the medium and low reduced damping range. Both numerical calculations are in fairly good agreement, which was to

be expected since they are both two-dimensional models, and have the same deficiencies for the prediction of physics which are clearly three-dimensional.

The flow over a cylinder undergoing forced oscillations has also been studied in comparison to the aeroelastic solutions. Similarly to other studies[17, 26] the phenomenon of "lock in" is observed for a range of forcing frequencies $\omega_f$ slightly above and below the natural vortex shedding frequency of the stationary cylinder. Differences in the topology of the wake were also observed, and will be the object of a further study.

**Computer Requirements**

Most of the calculations in this paper used a $384 \times 96$ structured mesh, divided into a number of subdomains that ranged from 12 to 16. Each subdomain was assigned to a different processor of an IBM SP2 Parallel computer, all of which collaborated to speed up the solution of the problem via explicit message passing accomplished with the MPI standard. In general, 40 multigrid cycles per time step were used in order to get a well converged solution at the end of each time step, and 36 steps per oscillation period were taken. With these parameters, a complete oscillation period requires about 14 minutes on 12 processors.

In contrast, when calculations were performed on a single node of an IBM SP1 System (equivalent to an RS6000/580) workstation, a complete cycle can be computed in 100 minutes.

It must be noted that the parallelization of the code is a key enabling technology required to obtain almost immediate feedback on the behavior of the code. In the future, improvements to the parallel program will be made, in order to be able to use larger computational meshes and produce solutions in a similar amount of time.

The implicit time stepping method, together with the parallel implementation of the algorithm make this method an extremely efficient tool to perform unsteady viscous calculations. In fact, without these improvements to the method, computation of fully resolved three-dimensional unsteady flows would not be a possibility in the near future.

## Conclusions

A fast, accurate solver for the unsteady Navier-Stokes equations has been developed, and preliminary results have been presented. The computational efficiency is two orders of magnitude higher than the equivalent explicit method for the same problem. The method can compute the wake and vortex shedding flows behind bluff bodies with great accuracy, and can resolve the details of the unsteady flow field. The improved artificial dissipation constructions of[12] are shown to yield more accurate shock resolution for transonic viscous flows. Initial aeroelastic results suggest that this solver can be coupled with a two-dimensional aeroelastic model as in,[3] in order to obtain flutter boundaries for airfoils representing an outboard section of a transonic swept wing. Furthermore, the parallel implementation of the algorithm scales rather well for a given mesh, and facilitates (due to reduced feedback cycle times) the understanding of unsteady viscous flows.

## Acknowledgment

This work has benefited from the generous support of ARPA under Grant No. N00014-92-J-1796 and AFOSR under Grant No. AFOSR-91-0391. Computational time on the NAS SP2 system was provided as a part of the IBM-CRA initiative.

## References

[1]Brenneis, A. and Eberle, A., "Application of an Implicit Relaxation Method Solving the Euler Equations for Time-Accurate Unsteady Problems," Journal of Fluids Engineering, Vol. 112, pp. 510-520, December 1990.

[2]Jameson, A., "Time Dependent Calculations Using Multigrid, with Applications to Unsteady Flows Past Airfoils and Wings," AIAA Paper 91-1596, June 1991.

[3]Alonso, J. J. and Jameson, A., "Fully-Implicit Time-Marching Aeroelastic Solutions", AIAA Paper 94-0056, AIAA 32nd Aerospace Sciences Meeting, Reno, NV, January 1994.

[4]Melson, N. D., Sanetrik, M. D., and Atkins, H. L.,"Time-Accurate Navier-Stokes Calculations with Multigrid Acceleration", Procs. of the Sixth Copper Mountain Conference on Multigrid Methods, Copper Mountain, Colorado, April, 1993.

[5]Arnone, A., Liou, M. S., and Povinelli, L. A., "Multigrid Time-Accurate Integrations of Navier-Stokes Equations," 24th Fluid Dynamics Conference, July 1993, Orlando, Florida, AIAA Paper 93-3361.

[6]Arnone, A., "On the Use of Multigrid in Turbomachinery Calculations," Proceedings of the International Workshop on Solution Techniques for Large-Scale CFD Problems, W.G. Habashi, Editor, Montreal, September, 1994.

[7]Tatsumi, S., Martinelli, L., and Jameson, A., "Design, Implementation, and Validation of Flux Limited Schemes for the Solution of the Compressible Navier-Stokes Equations", AIAA Paper 94-0647, AIAA 32nd Aerospace Sciences Meeting, Reno, NV, January 1994.

[8]Martinelli, L., "Calculation of Viscous Flows with a Multigrid Method," Ph.D. Dissertation, Mechanical & Aerospace Engineering Department, Princeton University, October, 1987.

[9]Martinelli, L. and Jameson, A., "Validation of a Multigrid Method for the Reynolds Averaged Equations," AIAA Paper 88-0414, AIAA 26th Aerospace Sciences Meeting, Reno, NV, January, 1988.

[10]Liu, F. and Jameson, A., "Multigrid Navier-Stokes Calculations for Three-Dimensional Cascades," AIAA Paper 92-0190, AIAA 30th Aerospace Sciences Meeting, Reno, NV, January, 1992.

[11]Baldwin, B. S. and Lomax, H., "Thin Layer Approximation and Algebraic Model for Separated Turbulent Flows," AIAA Paper 78-0257, 1978.

[12]Jameson, A., "Artificial Diffusion, Upwind Biasing, Limiters, and their Effect on Accuracy and Multigrid Convergence in Transonic and Hypersonic Flow," presented at the AIAA 11th Computational Fluid Dynamics Conference, Orlando, July 1993.

[13]Jameson, A., "Analysis and design of numerical schemes for gas dynamics 2, artificial diffusion and discrete shock structure," Int. J. of Comp. Fluid Dyn., To Appear.

[14]Bisplinghoff, R. L., Ashley, H. and Halfman, R. L., Aeroelasticity, Addison-Wesley, Reading, Massachusetts, 1955.

[15]Dowell, E. H., Curtiss, H. C., Scanlan, R. H. and Sisto, F., A Modern Course in Aeroelasticity, Sijthoff and Noordhoff, Alphen ann den Rijn, The Netherlands, 1978.

[16]Schlichting, H., Boundary Layer Theory, 7th Edition, McGraw-Hill, 1979.

[17]Blackburn, H. M., and Karniadakis, G. E., "Two- and Three- Dimensional Vortex-Induced Vibration of a Circular", ISOPE-93 Conference, Singapore, 1993.

[18]Belov, A., Martinelli, L., and Jameson, A., "A New Implicit Algorithm with Multigrid for Unsteady Incompressible Flow Calculations," AIAA Paper 95-0049, AIAA 33rd Aerospace Sciences Meeting, Reno, NV, January, 1995.

[19]"MPI: A Message-Passing Interface Standard," Message Passing Interface Forum, March, 1994.

[20]Alonso, J. J., Mitty, T. J., Martinelli, L., and Jameson, A.,"A Two-Dimensional Multigrid-Driven Navier-Stokes Solver for Multiprocessor Architectures," Presented at the Parallel CFD '94 Conference, Kyoto, Japan, May 1994.

[21]Williamson, C. H. K.,"Defining a Universal and Contiguous Strouhal-Reynolds Number Relationship for the Laminar Vortex Shedding of a Circular Cylinder," Physics of Fluids, 31:2742–2744, October, 1988.

[22]König, M., Eisenlohr, H., and Eckelmann, H. "The Fine Structure in the Strouhal-Reynolds Number Relationship of the Laminar Wake of a Circular Cylinder," Physics of Fluids, 2:1607–1614, September, 1990.

[23]Hammache, M. and Gharib, M., "An Experimental Study of the Parallel and Oblique Vortex Shedding from Circular Cylinders," Fluid. Mech., 232:567–590, 1991.

[24]Griffin, O. M., "Vortex-Induced Vibrations of Marine Structures in Uniform and Sheared Currents," NSF Workshop on Riser Dynamics, University of Michigan, 1992.

[25]Tatsumi, S, Martinelli, L., and Jameson, A.,"A New High Resolution Scheme for Compressible Viscous Flows with Shocks," AIAA Paper 95-0466, AIAA 33rd Aerospace Sciences Meeting, Reno, NV, January, 1995.

[26]Mittal, S. and Tezduyar,T. E., "A Finite Element Study of Incompressible Flows Past Oscillating Cylinders and Aerofoils," International Journal for Numerical Methods in Fluids, vol. 15, 1073-1118, 1992.

[27]Venkatakrishnan, V.,"Computation of Unsteady Transonic Flows over Moving Airfoils," Ph.D. Dissertation, Dept. of Mechanical and Aerospace Engineering, Princeton University, October 1986.

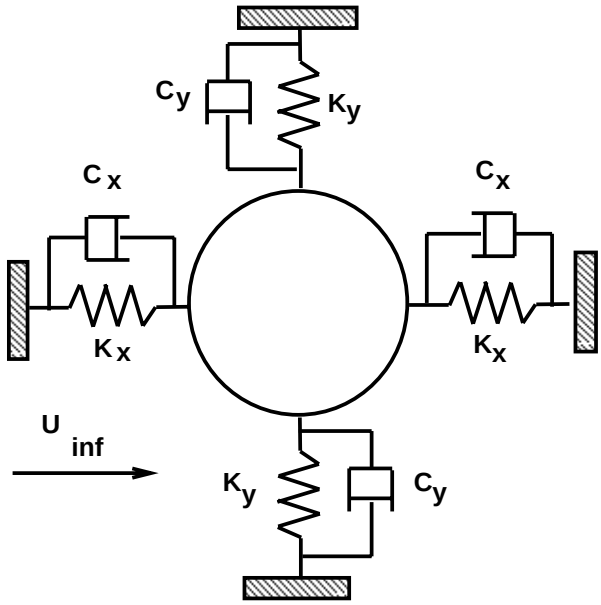


**Fig. 1 Aeroelastic Model for Cylinder Self-Induced Vibrations.**

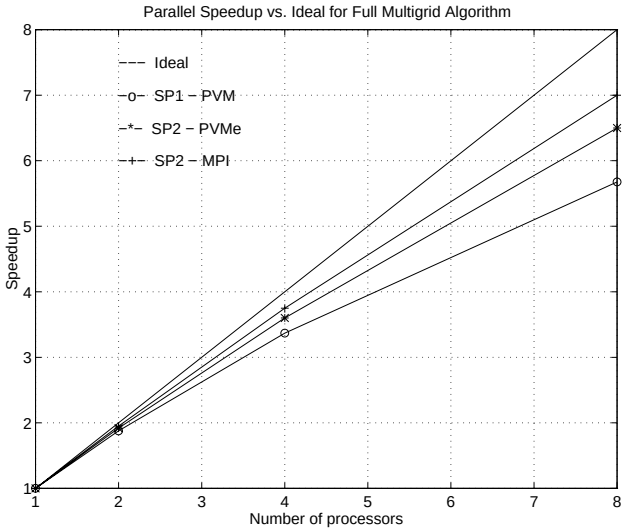


**Fig. 2 Parallel Speedup for UFLO82NSP for Different Message Passing Standards on Two Different Platforms.**

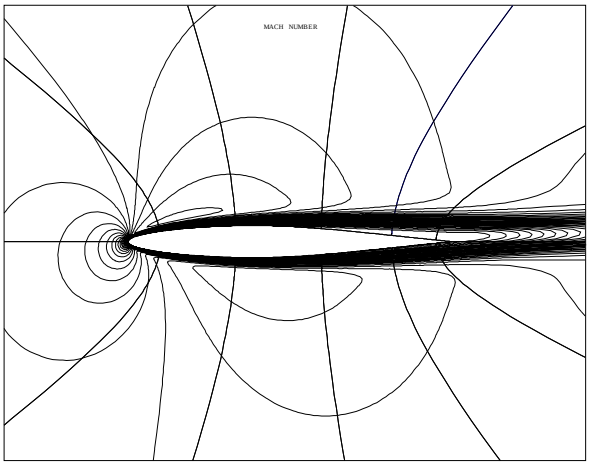


**Fig. 3 NACA 64A010 airfoil at $2^\circ$ angle of attack, $Re_\infty = 5000$. Radial lines show interprocessor boundaries.**

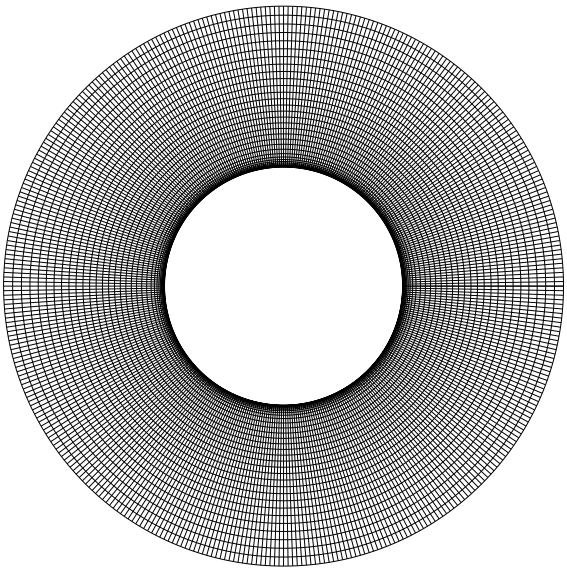

**Fig. 4 Detail of the O-mesh for Unsteady Calculations.**

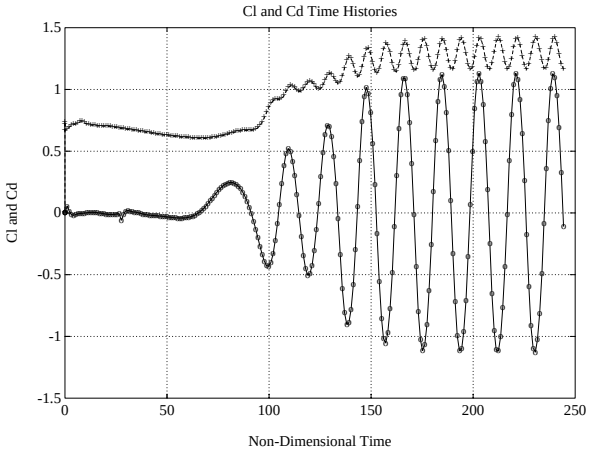


**Fig. 5 Time History of the Coefficients of Lift and Drag.**

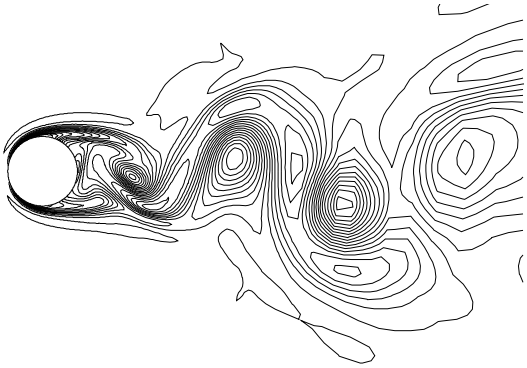

**Fig. 6 Entropy Contours in the Flow Field.**

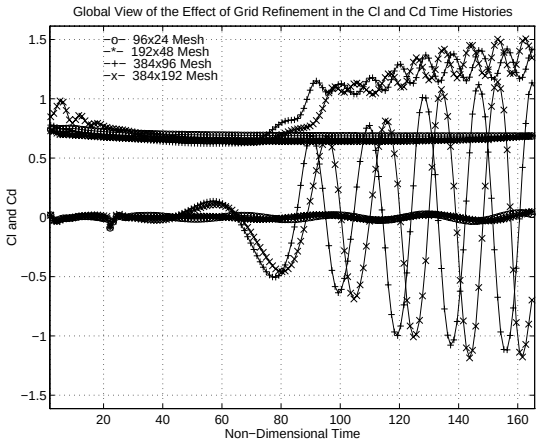


**Fig. 7 Time Histories of $C_l$ and $C_d$ for the Grid Refinement Study.**

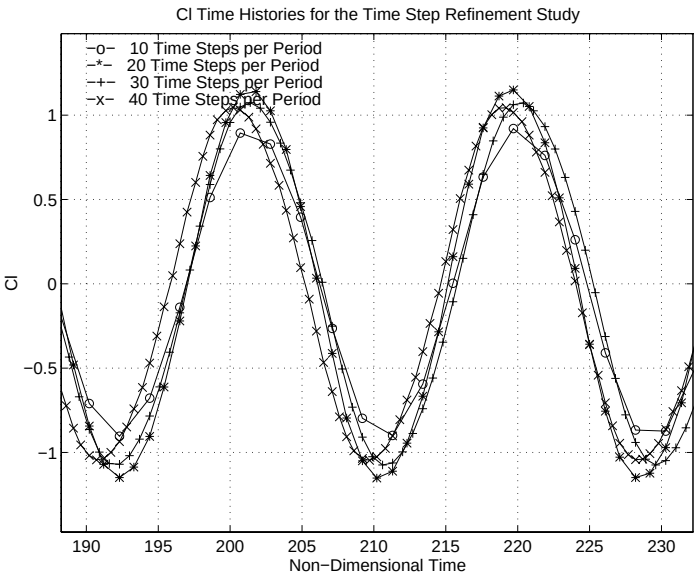


**Fig. 8 Time Histories of $C_l$ for the Time Step Refinement Study.**

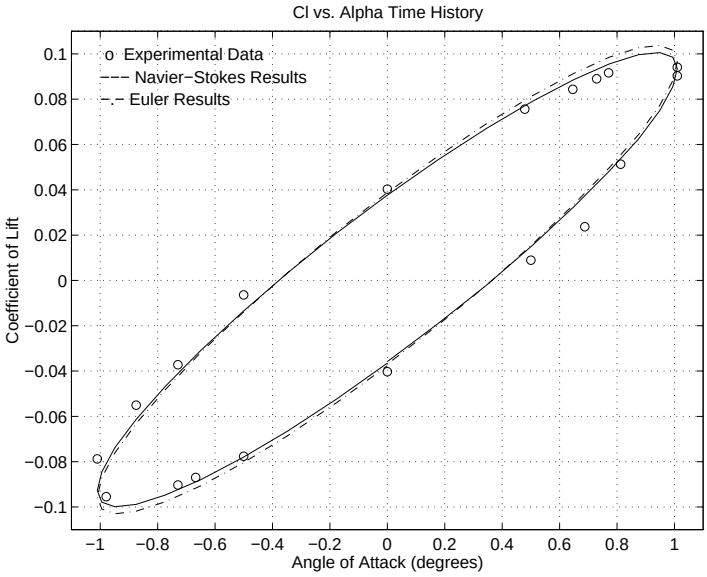


**Fig. 9 Coefficient of Lift Time History.**

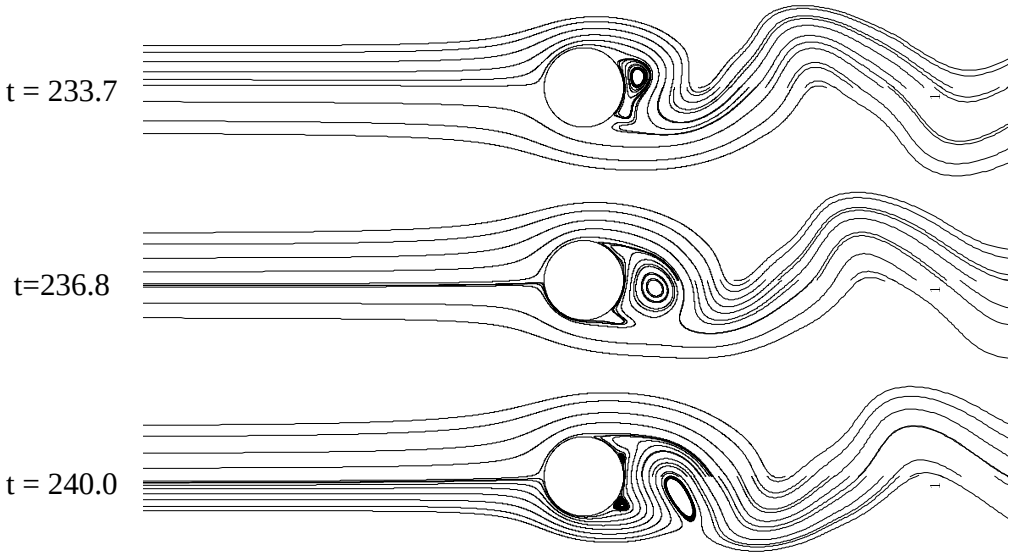


**Fig. 10 Instantaneous Streamlines at Three Different Times in the Vortex Shedding Process.**

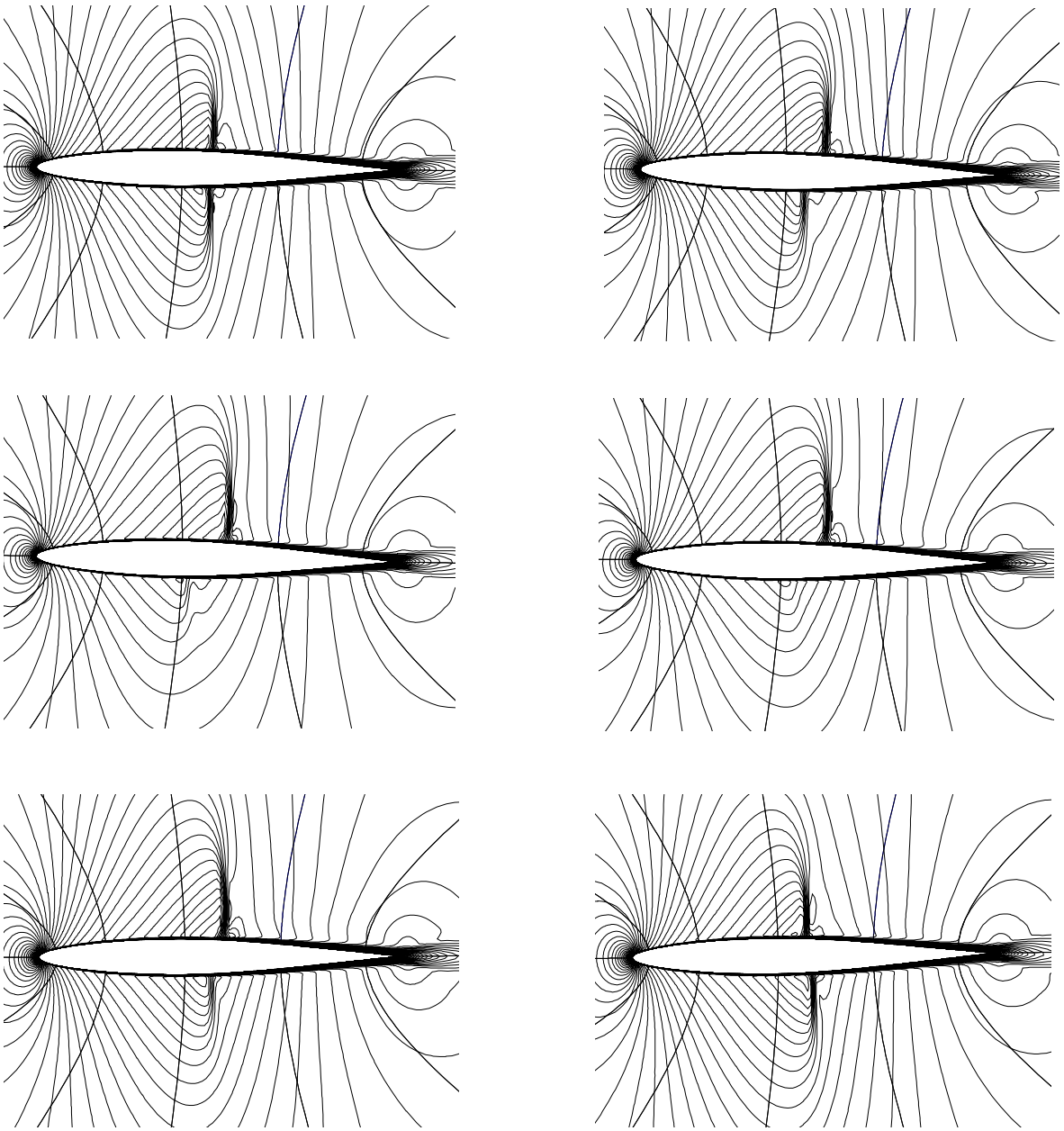

**Fig. 11 Mach Number Contours. Pitching Airfoil Case.** $Re = 1.0 \times 10^6$, $M_\infty = 0.796$, $K_c = 0.202$. **Read figures by lines.**

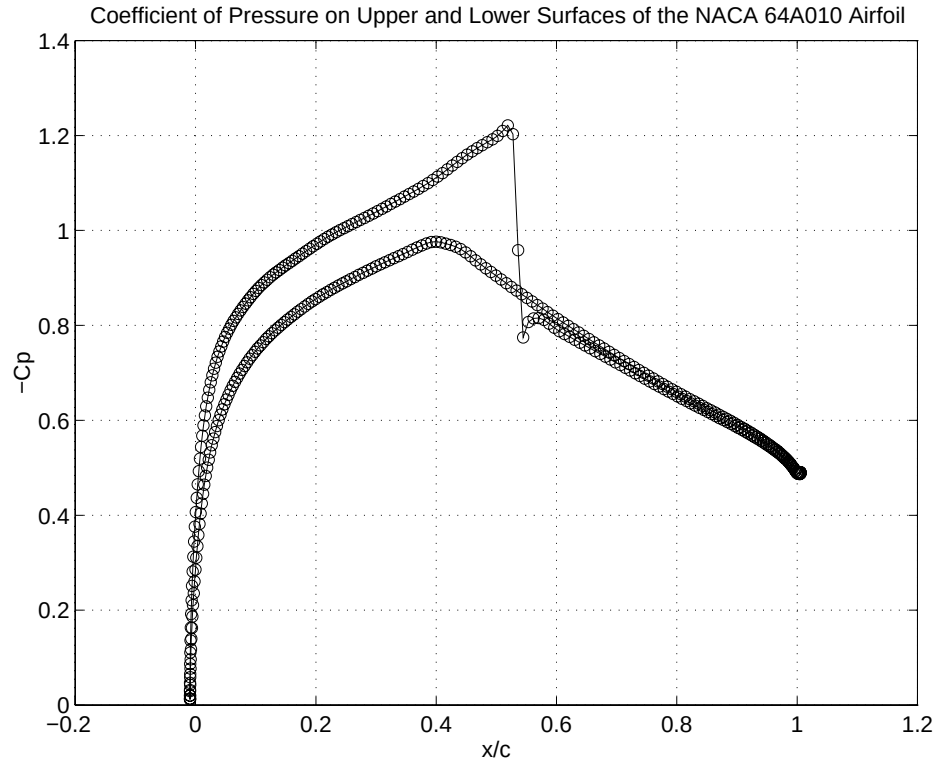


**Fig. 12 Coefficient of Pressure on a Grid Line Just Outside of the Boundary Layer.**

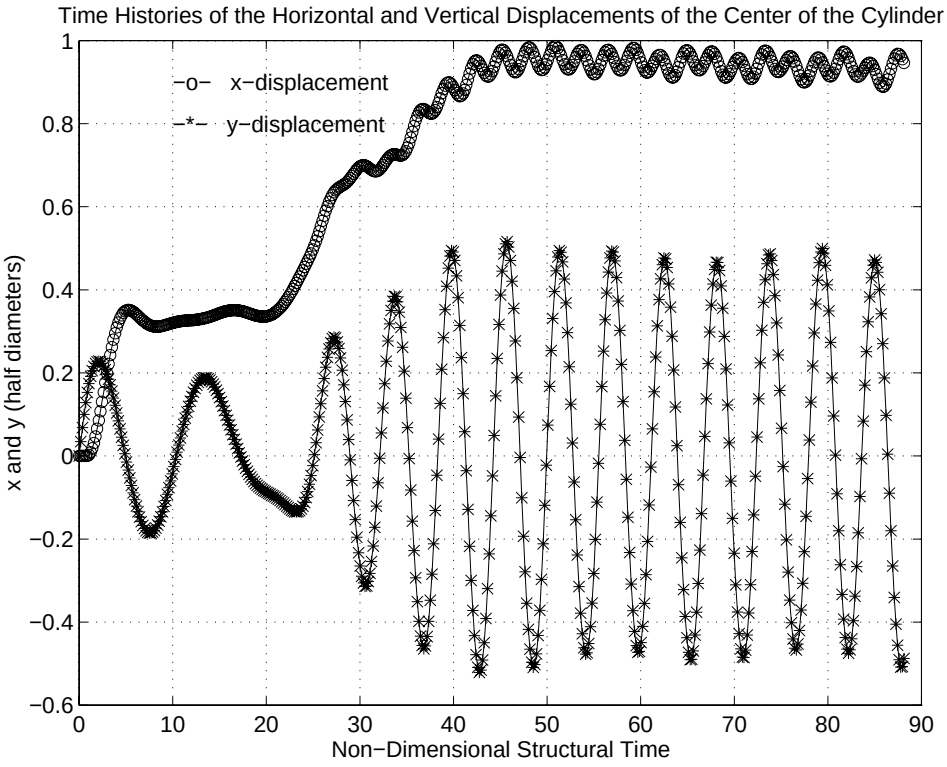


**Fig. 13 Time Evolution of the Coordinate Displacements for $\frac{\zeta}{\mu} = 5.0$.**

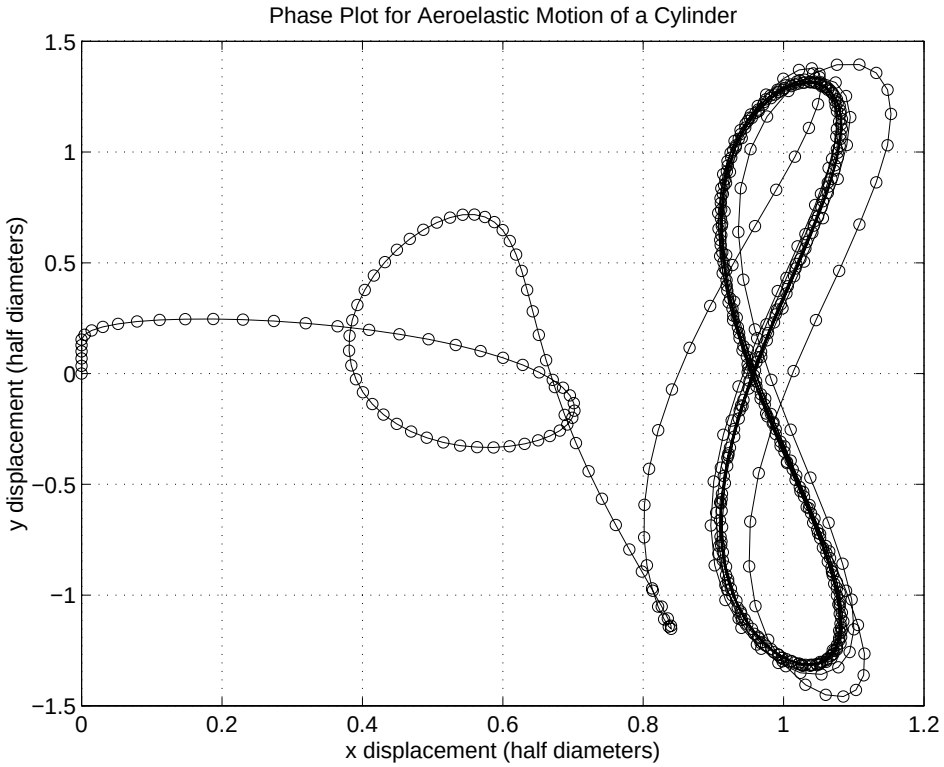


**Fig. 14 Phase Plot for the Aeroelastic Motion of a Circular Cylinder.**

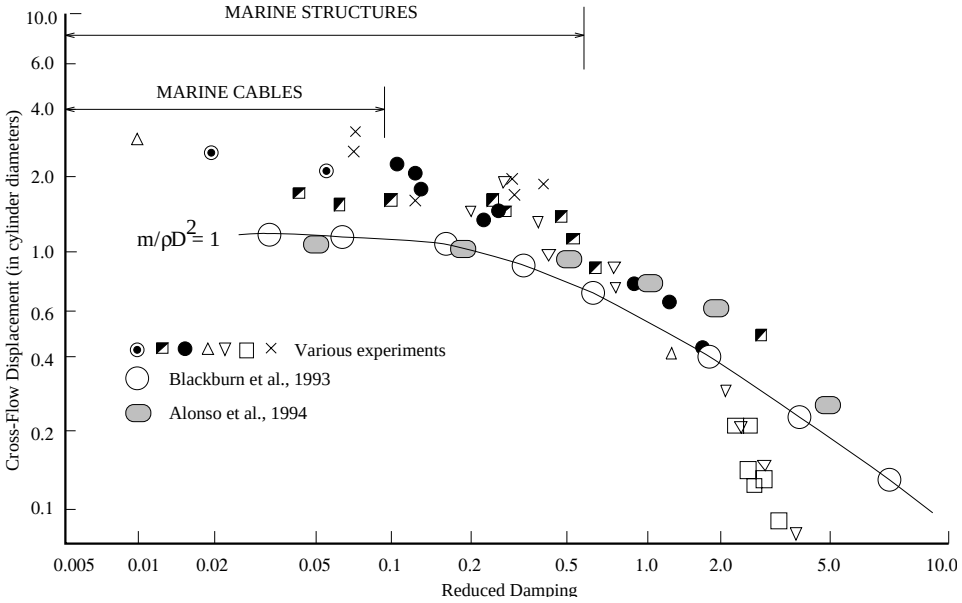


**Fig. 15 Maximum Cross Flow Displacement (in Cylinder Diameters) for Several Experimental Results, Blackburn et al., and the present method for $\mu = 5.0$.**